

Ternary Polymer Solar Cells with High Efficiency of 14.24% by Integrating Two Well-Complementary Nonfullerene Acceptors

Huanxiang Jiang, Xiaoming Li, Jianing Wang, Shanlin Qiao, Yong Zhang,* Nan Zheng, Weichao Chen,* Yonghai Li,* and Renqiang Yang*

Ternary polymer solar cells (PSCs) are one of the most promising device architectures that maintains the simplicity of single-junction devices and provides an important platform to better tailor the multiple performance parameters of PSCs. Herein, a ternary PSC system is reported employing a wide bandgap polymeric donor (PBTA-PS) and two small molecular nonfullerene acceptors (labeled as LA1 and 6TIC). LA1 and 6TIC keep not only well-matched absorption profiles but also the rational crystallization properties. As a result, the optimal ternary PSC delivers a state of the art power conversion efficiency (PCE) of 14.24%, over 40% higher than the two binary devices, resulting from the prominently increased short-circuit current density (J_{sc}) of 22.33 mA cm^{-2} , moderate open-circuit voltage (V_{oc}) of 0.84 V, and a superior fill factor approaching 76%. Notably, the outstanding PCE of the ternary PSC ranks one of the best among the reported ternary solar cells. The greatly improved performance of ternary PSCs mainly derives from combining the complementary properties such as absorption and crystallinity. This work highlights the great importance of the rational design of matched acceptors toward highly efficient ternary PSCs.

PSCs in practical applications.^[1,6–11] Moreover, device optimization including interfacial and device engineering also plays a crucial role in promoting the development of PSCs.^[12–17] Nevertheless, restrained by the prerequisite molecular energy level differences of the donor and acceptor materials, the conventional binary PSCs built with one donor–acceptor pair can hardly harvest the solar photons as much as possible in a wide range of solar spectrum.^[18,19] Consequently, ternary PSCs composed of three photovoltaic materials and maintaining the simplicity of fabrication have emerged as a promising approach to solve this dilemma.^[20–24]

Originally, ternary PSCs were mainly fabricated based on two polymer donors and one fullerene acceptor.^[20,25] For example, Sun and co-workers combined two efficient polymer donors (PTB7-Th and PDBT-T1) into the ternary system.

The resulting ternary solar cells with PC₇₁BM as the acceptor exhibited further enhanced efficiency up to 10.2% compared to the binary counterparts.^[23] However, elaborately manipulating the morphologies of bulk heterojunction (BHJ) containing two conjugated polymers still remains an obstacle. Fortunately, the report of small molecular nonfullerene acceptors since 2015 offers a more flexible choice of materials and enables ternary PSCs to move forward on a new journey.^[26] Ternary solar cells composed of one medium bandgap donor,


1. Introduction

Polymer solar cells (PSCs) have been a research hotspot due to their advantage of solution processing, flexibility, and semi-transparency.^[1–5] Promoted by the prosperous development of small molecular nonfullerene acceptors and diverse donor materials, the power conversion efficiencies (PCE) of polymer solar cells have exceeded 14%, suggesting the bright promise of

H. Jiang, X. Li, Dr. Y. Li, Prof. R. Yang
CAS Key Laboratory of Bio-based Materials
Qingdao Institute of Bioenergy and Bioprocess Technology
Chinese Academy of Sciences
Qingdao 266101, China
E-mail: liyh@qibebt.ac.cn; yangrq@qibebt.ac.cn

H. Jiang
Center of Materials Science and Optoelectronics Engineering
University of Chinese Academy of Sciences
Beijing 100049, China

I. Li, Dr. S. Qiao
College of Chemistry and Pharmaceutical Engineering
Hebei University of Science and Technology
Shijiazhuang 050018, China

 The ORCID identification number(s) for the author(s) of this article can be found under <https://doi.org/10.1002/adfm.201903596>.

J. Wang, Prof. Y. Zhang
Institute of Optoelectronic Materials and Technology
South China Normal University
Guangzhou 510631, China
E-mail: zycq@scnu.edu.cn

Dr. N. Zheng
Institute of Polymer Optoelectronic Materials and Devices
State Key Laboratory of Luminescent Materials and Devices
South China University of Technology
Guangzhou 510640, China

Dr. W. Chen
College of Textiles & Clothing
State Key Laboratory of Bio-fibers and Eco-textiles
Collaborative Innovation Center for Eco-Textiles of Shandong Province
Qingdao University
Qingdao 266071, China
E-mail: chenwc@qdu.edu.cn

DOI: 10.1002/adfm.201903596

one fullerene acceptor, and one nonfullerene small molecular acceptor were fabricated as well.^[27,28] The fullerene acceptors featured with high electron mobility and well miscibility are usually expected to maintain the favorable charge transport and BHJ morphologies. The nonfullerene acceptors featured with high extinction coefficient and broad absorption spectra are utilized as the third component to enhance the light harvesting ability of the ternary BHJ blends. Benefit from the fine-tuned morphology, improved charge transport, and efficient energy transfer between the nonfullerene acceptor and fullerene acceptor, excellent PCEs over 12% were recorded from this type of ternary solar cells.^[24,29] The isotropy charge transfer property of fullerene derivatives could help maximize the charge extraction. However, the intrinsic drawbacks of fullerene derivatives including the inferior extinction coefficient and poor energy level adjustability are not conducive to PSCs toward the state-of-the-art efficiencies.^[20,30,31] As a contrast, the absorption properties and energy levels of nonfullerene acceptors can be finely tuned through ingenious molecular design. In addition, the energy losses (defined as $E_{\text{loss}} = E_{\text{g}}^{\text{pt}} - qV_{\text{OC}}$, where E_{g} refers to the bandgap of donor or acceptor whichever has a smaller bandgap, usually calculated from the onset of external quantum efficiency curves, V_{OC} is the open-circuit voltage, and q is elementary charge) in nonfullerene-based PSCs can be alleviated because of the low driving force for charge separation.^[32–34] To avoid deep charge traps and reduce energy loss, the lowest unoccupied molecular orbitals (LUMO) energy levels of two acceptors should be close in ternary PSCs.^[34,35] Moreover, it is known that the dynamics of exciton dissociation and charge transport greatly depend on the compatibility of the materials.^[18,56] Fortunately, the versatile acceptor–donor–acceptor (A–D–A) type nonfullerene acceptors share similar chemical structure, promising with good compatibility between acceptors and providing a wide range of material combination that could offer broadened photon harvesting and finely matched energy levels. Beneficial from the aforementioned multiple advantages of nonfullerene acceptors, ternary solar cells fabricated from one donor and two nonfullerene acceptors have demonstrated great potential to increase the efficiencies of solar cells with PCE over 13.5%.^[37] For example, Hou integrated two chlorinated narrow bandgap acceptors IT-2Cl and IT-4Cl into the ternary PSCs with PBDB-TF as the donor. The resulting ternary solar cells demonstrated the best PCE of 14.18% with high short-circuit current density (J_{SC}) over 22 mA cm⁻² and FF over 76%.^[38] Recently, ternary solar cell with PCE of 14.13% was fabricated from donor PM6 (PBDB-TF) and two structurally similar acceptors with similar absorption spectra and different crystallinity. The adorable efficiency was mainly contributed by the outstanding fill factor over 78% originating from the well-tuned morphology and molecular orientations.^[38,39] Therefore, elaborate selection of a suitable third component with complementary basic properties is critical for the development of high-performance ternary solar cells.

In our previous work, we fabricated a high-efficiency ternary blend PSC by combining a new medium bandgap polymer PBTA-PS and two structural similar acceptors (6TIC and IT-4F). The ternary PSC displayed a higher PCE of 13.27% than PBTA-PS:ITIC (IT-4F) binary solar cells.^[40] Very recently, we reported an effective but simple approach to balance the crystallinity of

acceptors and miscibility with donors. That is, a simple phenyl was introduced to the tail of alkyl side chain of acceptor whereby we reported a new acceptor IDIC-C4Ph (labeled as LA1 here).^[41] The crystallinity of IDIC-C4Ph (LA1) was slightly weakened which contributed to remarkably improved heterojunction morphologies and orderly stacking orientations. However, the absorption range of LA1 was narrow with the onset wavelength of 765 nm, which restrained the further improvement of J_{SC} and efficiencies. Thus, in this contribution, we built ternary solar cells based on this promising acceptor LA1. Here, the medium bandgap polymer PBTA-PS was utilized as the donor. And from the primary point of absorption complementary and the match of energy levels, a nonfullerene acceptor 6TIC with strong absorption in near-infrared (NIR) range and modest energy levels was adopted as the third component for ternary solar cells.^[42] The PBTA-PS:LA1 host binary PSCs exhibit moderated efficiency of 10.22% with inferior J_{SC} of 15.17 mA cm⁻² and decent FF over 75%. Exhilaratingly, after the addition of 6TIC, the photo response of the ternary solar cells is greatly expanded, contributing to the significantly increased J_{SC} up to 22.33 mA cm⁻². Concurrently, impressive FF approaching 76% was maintained in the ternary devices, similar with LA1-based binary solar cells. As a consequence, the optimal ternary PSCs deliver a state of the art PCE of 14.24%, which is over 40% higher than LA1 (10.22%)- and 6TIC (8.15%)-based binary PSCs. Overall, we have reported a high-performance ternary PSC system and highlighted the importance of rational selection of acceptors with well complementary properties.

The chemical structures of the donor material PBTA-PS, acceptor LA1, and 6TIC are displayed in **Figure 1a**. The absorption spectra of the thin films and energy level alignment are shown in Figure 1b,c, respectively. These materials possess well-matched absorption profiles between 400 and 900 nm, which is fairly important for ternary solar cells to cover a broad range of solar spectrum and harvest photons as much as possible. It is worth noting that the photoluminescence (PL) spectrum of LA1 strongly overlaps with the absorption spectrum of 6TIC, indicating there is a possible energy transfer process from LA1 to 6TIC. To verify this, PL of neat LA1, 6TIC, and their blend films were conducted. The neat LA1 film exhibits an intense PL emission at 748 nm while the neat 6TIC film exhibits a relatively weak emission intensity at 817 nm. After blending LA1 with 6TIC, the characteristic PL peak of LA1 completely disappeared with a slightly enhanced emission of 6TIC (Figure S1a, Supporting Information), indicative of the efficient energy transfer from LA1 to 6TIC. Therefore, a possible channel to generate charges of LA1 excitons can be formed via such an energy transfer to 6TIC. After blending with donor PBTA-PS, the PL of PBTA-PS was thoroughly quenched in the ternary system (Figure S1b, Supporting Information), indicating effective charge generation between PBTA-PS and acceptors.^[43,44]

The highest occupied molecular orbitals (HOMO) energy levels of PBTA-PS, LA1, and 6TIC lie on -5.34, -5.70, and -5.45 eV and LUMO energy levels were determined to be -3.40, -3.93, and -3.94 eV, respectively. As the energy level alignment are not appropriate for charge transfer between acceptors, acceptor-only devices were fabricated to determine the possibility of charge transfer between acceptors with the device configuration

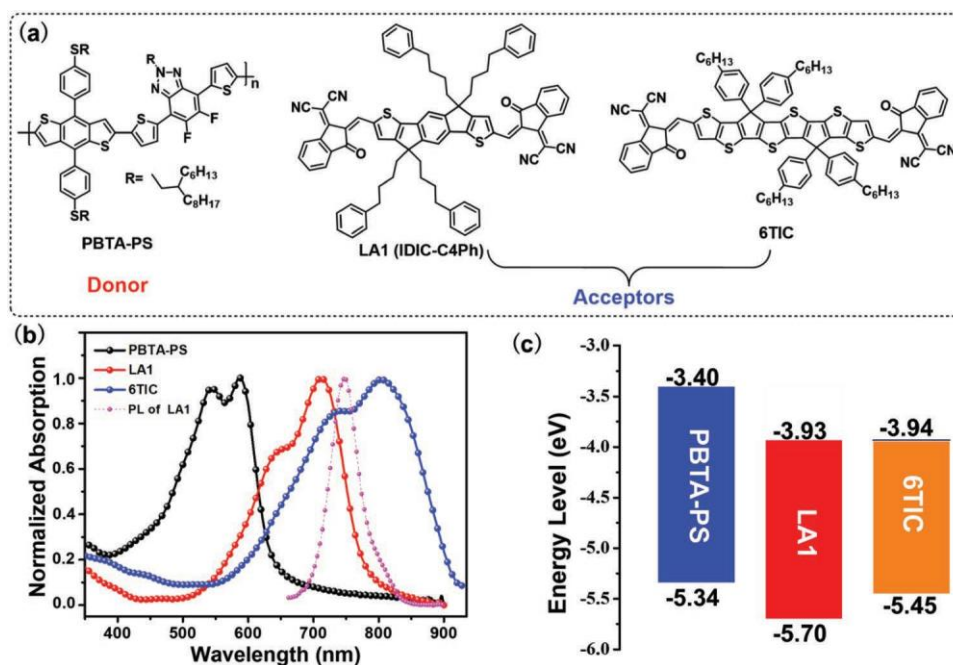


Figure 1. a) Chemical structures of PBTA-PS, LA1, and 6TIC. b) Normalized absorption spectra of neat PBTA-PS, LA1, 6TIC films and normalized photoluminescence (PL) emission spectrum of neat LA1 film. c) Energy level diagrams of PBTA-PS, LA1, and 6TIC.

of indium tin oxides (ITO)/poly(3,4-ethylenedioxythiophene):poly(styrenesulfonate) (PEDOT:PSS)/acceptors/perylene diimide functionalized with amino N-oxide (PDINO)/aluminum (Al). As shown in Figure S2 in the Supporting Information, the devices based on neat LA1 and 6TIC films generated low J_{SC} of 0.43 and 0.72 mA cm⁻², respectively. LA1:6TIC device exhibits a smaller J_{SC} of 0.65 mA cm⁻² than 6TIC neat device, revealing negligible charge transfer between LA1 and 6TIC.^[45] To further Besides, the high lying LUMO energy levels of LA1 and 6TIC locate at similar positions, which could help to obtain high V_{OC} s in the binary and ternary systems.

2D grazing incidence X-ray diffraction (2D-GIXD) measurements were further carried out to investigate the molecular packing and orientations of neat films. The 2D-GIXD patterns and the corresponding in-plane (IP) and out-of-plane (OOP) line cuts of three neat films and the blend of two acceptors are depicted in **Figure 2**. In the IP direction, neat PBTA-PS, LA1, and 6TIC films exhibit intense (100) diffraction peaks at $q_{xy} \approx 0.22, 0.40, \text{ and } 0.46 \text{ \AA}^{-1}$ and the corresponding lamellar distances are calculated to be 28.54, 15.72, and 13.65 Å, respectively. In the OOP direction, the (010) diffraction peaks of PBTA-PS, LA1, and 6TIC locate at $q_z \approx 1.71, 1.84, \text{ and } 1.82 \text{ \AA}^{-1}$, corresponding to the π - π stacking d-spacing of 3.67, 3.41, and 3.45 Å, respectively. Notably, three pure films exhibit a dominant face-on molecular orientation, which is advantageous for charge transport in the direction relative to charge collection. Additionally, in the OOP direction, LA1 shows sharper π - π stacking diffraction peaks, demonstrating a relatively strong crystallization propensity than 6TIC. The differential crystallization behavior of two acceptors leaves ample room for the morphology modulation of the ternary BHJ blends. Besides, the intrinsic (100) diffraction peak and (010) diffraction peak were detected from the LA1+6TIC blend, indicating 6TIC could

mix with LA1 intimately without devastating the preferred molecular packing orientations.

Conventional PSCs with a structure of ITO/PEDOT:PSS/donor: acceptors PDINO/Al were fabricated to evaluate the photovoltaic performance of the binary and ternary solar cells. The detailed optimization procedure including donor: acceptor weight ratios, thermal annealing, and additive process are collected in Tables S1–S3, Figure S3 in the Supporting Information. After adding 1% diphenyl ether (DPE) into the PBTA-PS:LA1 system, the V_{OC} slightly increased. On the contrary, after adding 1% DPE into the PBTA-PS:6TIC system, the V_{OC} dropped. Though the V_{OC} is mainly determined by the energy level differences of the HOMO level of donor and LUMO level of acceptors, the morphology and microstructure of blend film could also influence V_{OC} .^[46] As the additives may tailor the changes of V_{OC} in different systems, it is difficult to predict how the additive influences the V_{OC} .^[47,48] In this work, we consider that the variations of V_{OC} may be partly correlated with the evolutions of BHJ morphologies with or without DPE (Figure S4, Supporting Information). The current density–voltage (J - V) curves of binary and ternary devices under optimal conditions are illustrated in **Figure 3** and the corresponding detailed photovoltaic parameters are listed in **Table 1**. Distinctively, the LA1-based binary solar cells delivered an optimal PCE of 10.22%, with a low J_{SC} of 15.17 mA cm⁻², and decent FF over 75%. From the EQE measurement, strong photo response at 600–700 nm is observed, which could be related to the excellent absorption property of LA1 as we previously reported.^[41] However, the photo response decreased sharply around 800 nm ascribed to the narrow absorption spectrum of LA1, leaving ample room for the broadening of light harvesting. Meanwhile, in spite of broad absorption of 6TIC, relatively low efficiency was detected from 6TIC-based binary solar cells with the highest PCE of

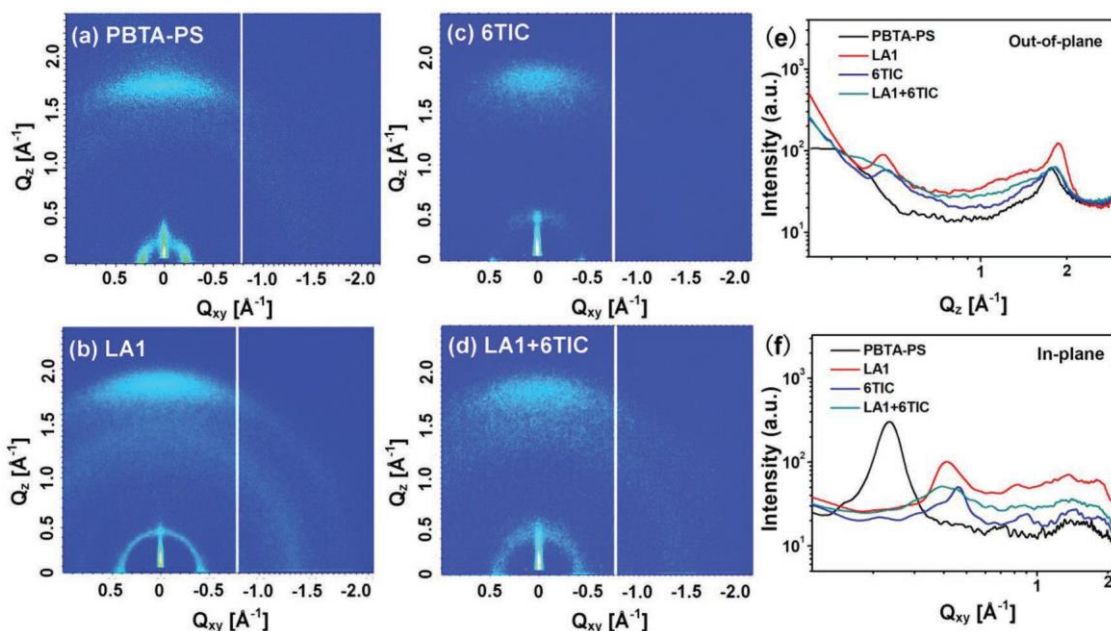


Figure 2. 2D-GIXD scattering patterns of a) PBTA-PS, b) LA1, c) 6TIC, and d) LA1+6TIC; the line profiles along the e) out of plane and f) in plane.

8.15%, mainly ascribed to the inferior FF of 62.32%. From the EQE curve of 6TIC-based binary device, broad photo response but low EQE values was found, accompanying with a low valley around 650 nm, resulting in the relatively low J_{SC} . Thus from the view of complementary of absorption or photo response, the two binary solar cells have great potential to improve the photovoltaic properties via the construction of ternary devices.

With 30% 6TIC (the weight ratio of 6TIC added to the acceptors, hereinafter), the as-cast ternary solar cells reached the best efficiency with the maximum PCE of 10.26%, higher than the as-cast or optimal PBTA-PS:LA1- and PBTA-PS:6TIC-based binary solar cells (see Tables S2 and S3). After introducing 2% DPE, the device performance reached optimum. The optimal ternary device delivered a best PCE of 14.24%, with a V_{OC} of

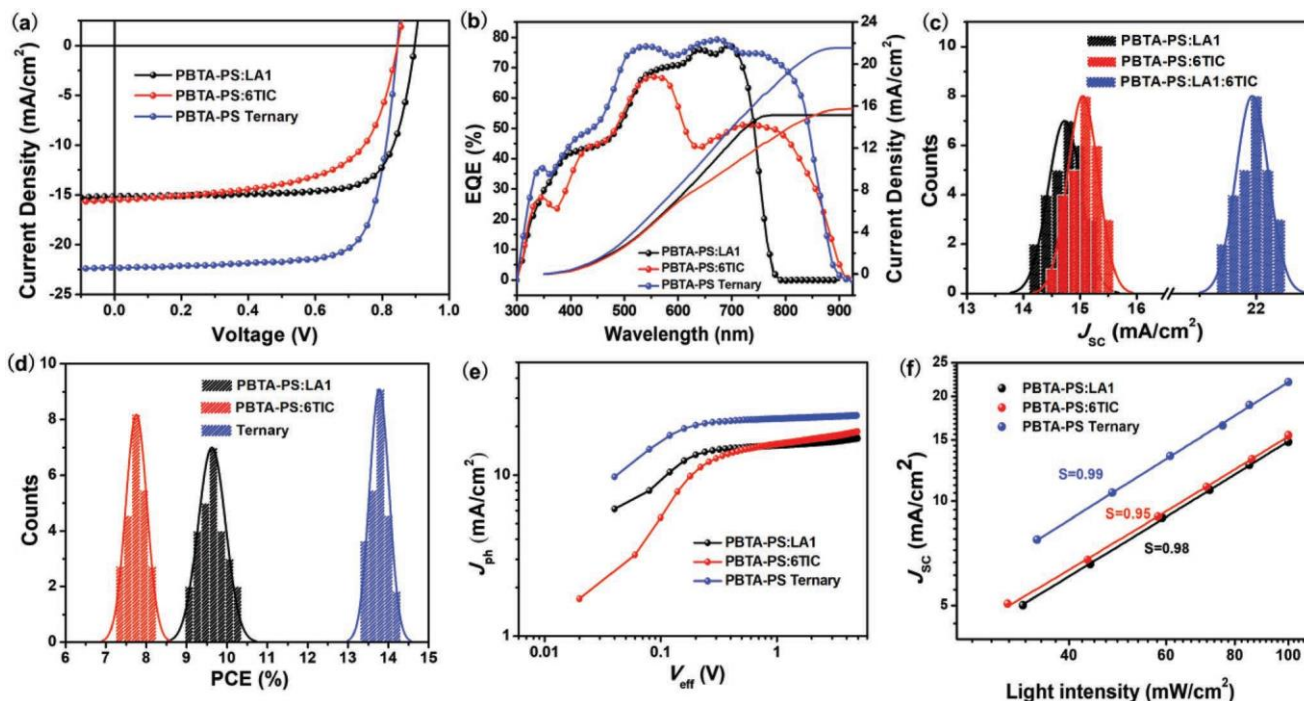


Figure 3. a) The optimal J - V curves of the binary and ternary solar cells; b) the respective EQE curves and the integrated current densities; c) statistical J_{SC} and d) PCE distribution histograms of the optimal binary and ternary devices based on at least 25 cells; e) photocurrent density versus effective voltage; f) plot of light intensity versus of J_{SC} of the optimal binary and ternary PSCs.

Table 1. The photovoltaic parameters of optimal binary and ternary PSCs.

| Active layers | V_{oc} [V] | J_{sc} | | FF [%] | PCE ^{b)} [%] | μ_e/μ_h 10^{-4} cm ² [V ⁻¹ s ⁻¹] |
|-----------------------------|-----------------------|-------------------------|---------------------|-------------------------|-------------------------|--|
| | | J_{sc} | $[J_{sc}^{EQE}]^a)$ | | | |
| | | [mA cm ⁻²] | | | | |
| PBTA-PS:LA1 (1.5% DPE) | 0.89 (0.89 ± 0.01) | 15.17 (14.84 ± 0.43) | 14.85 | 75.10 (74.93 ± 0.28) | 10.22 (9.56 ± 0.59) | 2.56/1.88 |
| PBTA-PS:6TIC (1% DPE) | 0.84 (0.84 ± 0.01) | 15.47 (15.23 ± 0.31) | 15.06 | 62.32 (59.93 ± 2.53) | 8.15 (7.84 ± 0.32) | 1.18/4.22 |
| PBTA-PS Ternary (2% DPE) | 0.84 (0.84 ± 0.01) | 22.33 (21.95 ± 0.36) | 21.64 | 75.94 (74.23 ± 1.57) | 14.24 (13.89 ± 0.31) | 5.42/4.21 |

^{a)}Integrated from the EQE spectrum; ^{b)}Average values with standard deviations were obtained from at least 25 cells.

0.84 V, J_{sc} of 22.33 mA cm⁻², and FF of 75.94%. From the EQE curves of ternary device, the low valley around 650 nm of 6TIC binary device was paved over, which could be attributed to the complementary absorption of LA1. Besides, the photo response from 750 to 900 nm was enhanced compared to the 6TIC binary system, which could be attributed to the optimized molecular packing, reduced recombination, and efficient charge transport of 6TIC. It is noteworthy that the V_{oc} of ternary system were pinned at the smallest V_{oc} of binary systems and hardly change with the composition, which might indicate that the acceptors adopted a cascade structure rather than an alloy structure (Figure S3 and Table S1, Supporting Information).^[49] Specifically, the statistical PCE distribution histograms of the optimal binary and ternary devices based on at least 25 cells are displayed in Figure 3d. The average PCE was determined to be 13.89% with a standard deviation of 0.31 from at least 25 individual devices (see Table 1).

The statistical J_{sc} distribution histograms are shown in Figure 3c to present a more intuitive illustration. The greatly improved J_{sc} of ternary devices could be attributed to the well-complementary light-harvesting properties of two acceptors together with the optimized morphology. Based on EQE integration versus the AM 1.5 G, the J_{sc}^{EQE} of PBTA-PS:LA1, PBTA-PS:6TIC, and ternary PSCs are confirmed to be 15.07, 15.68, and 21.59 mA cm⁻², respectively, consistent with measured J_{sc} (error < 5%).

As shown in Figure S5 in the Supporting Information, the J - V curves of optimal PBTA-PS:LA1 and ternary devices in dark have been plotted. Region 1 refers to the leakage current, region 2 stands for recombination current, and region 3 represents series resistance. The ternary device exhibits lower leakage current, indicating that the shunt resistance is larger than PBTA-PS:LA1 binary device. What's more, the PBTA-PS ternary device exhibits similar series resistance ($3.33 \wedge$ cm²) with that of PBTA-PS:LA1 binary device ($3.99 \wedge$ cm²), which agrees well with the high FF of PBTA-PS:LA1 and the ternary devices.

The electron and hole mobilities (μ_e and μ_h) of optimal binary and ternary devices were measured by the space charge-limited current (SCLC) method (Table 1 and Figure S6, Supporting Information). The electron-only and hole-only diodes adopted the device structures of ITO/zinc oxide (ZnO)/active layer/PDINO/Al and ITO/PEDOT:PSS/active layer/Au, respectively. The ternary blend film exhibits high electron and hole mobility (5.42×10^{-4} and 4.21×10^{-4} cm² V⁻¹ s⁻¹ for electron and hole mobility, respectively), accompanying with a more

balanced charge transport ($\mu_e/\mu_h = 1.28$), which is consistent with the favorable FF and J_{sc} . Besides, the electron mobility in ternary system is higher than that in PBTA-PS:6TIC system, which could partly explain the improved photo response at 750–900 nm.

Charge carriers generated from exciton dissociation process could either be extracted and collected at the electrodes or be eliminated through the recombination process. Therefore, charge dissociation and extraction process of optimal binary and ternary devices were further investigated by plotting photocurrent density (J_{ph}) versus effective voltage (V_{eff}) (Figure 3e). $J_{ph} = J_L - J_D$, where J_L and J_D refer to the current densities under illumination and dark condition, respectively.^[49] $V_{eff} = V_0 - V$, where V_0 is the voltage when $J_{ph} = 0$, and V is the applied voltage. As shown in Figure 3e, the J_{ph} of PBTA-PS:LA1 could reach saturation (J_{sat}) values at a low V_{eff} of 1 V, while PBTA-PS:6TIC hardly reaches a saturation regime even at a high V_{eff} over 4 V, illustrating the inferior efficiency of exciton dissociation, which could be one origin for the low FF and photo response. In ternary system, the J_{ph} could reach saturation at a low V_{eff} of 1 V, indicating most of the generated charges were driven to the electrodes. Besides, the ternary solar cells exhibit higher overall charge collection efficiency (calculated by J_{ph} / J_{ph}^{sat}) of 95% than PBTA-PS:LA1 (88%) and PBTA-PS:6TIC (83%) binary devices under short-circuit condition, indicating better exciton generating and charge collection, which could partly explain the enhanced photo response at the wavelength of 750–900 nm.^[50] To further investigate the charge recombination process, J_{sc} versus light intensity (P_{light}) was plotted, which follows the power-law dependence of $J_{sc} \propto P_{light}^\alpha$.^[51,52] The α approaching 1 indicates negligible bimolecular recombination. As shown in Figure 3f, the PBTA-PS ternary device exhibits a higher α of 0.99 than those of PBTA-PS:LA1 (0.98) and PBTA-PS:6TIC (0.95) binary devices, indicating low bimolecular recombination in the ternary system.

By integrating J - V curves and the onsets of EQE curves, the V_{oc} deficits of optimal binary and ternary PSCs could be obtained intuitively.^[53] As **Figure 4** shows, the V_{oc} deficits for PBTA-PS:LA1, PBTA-PS:6TIC, and ternary PSCs are determined to be 0.70, 0.52, and 0.54 V, respectively. Obviously, the V_{oc} deficit of the ternary device is similar with PBTA-PS:6TIC binary system and lower than the host PBTA-PS:LA1 binary system, which may be related to the smaller E_g resulting from the narrow bandgap acceptor 6TIC. The E_g of PBTA-PS:LA1 binary system is 1.59 eV, which is larger than the E_g of PBTA-PS:6TIC and ternary systems (1.36 and 1.38 eV). This could

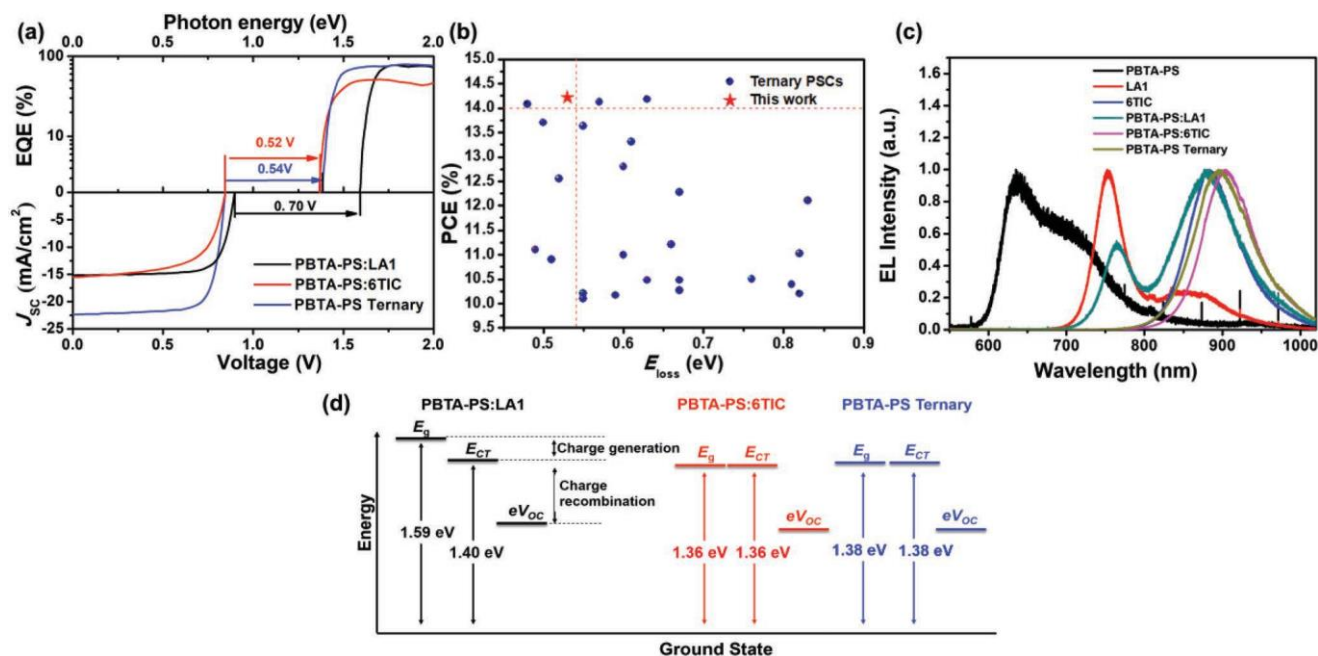


Figure 4. a) Combined plots of $J-V$ and EQE for the comparison of V_{OC} deficit from optimal binary and ternary PSCs; b) plots of PCE versus E_{loss} for reported ternary PSCs with PCE greater than 10%. Source references for the data points are provided in the Supporting Information. c) EL spectra of pristine and blend films. d) Schematic diagram of energy levels of binary and ternary PSCs.

partly explain that PBTA-PS:LA1 binary system could achieve high V_{OC} of 0.89 V while suffered from the high V_{OC} loss of 0.70 V.^[54] It is noteworthy that the E_{loss} of PBTA-PS:LA1:6TIC (0.54 eV) ranks one of the lowest among the reported high-efficiency ternary solar cells (see Figure 4b). Furthermore, the energy of charge transfer state (E_{CT}) was located to gain an insight into the energy loss channels. The energy loss E_{loss} can be divided into two parts, ΔE_1 and ΔE_2 . ΔE_1 ($E_g - E_{CT}$) takes place during the charge separation process while ΔE_2 ($E_{CT} - eV_{OC}$) occurs during charge recombination (Figure 4d). Electroluminescence (EL) measurement is an effective approach to locate the position of CTs. As shown in Figure 4c, the emission peaks at 780, 912, and 899 nm correlate to the EL emission of charge transfer states in PBTA-PS:LA1, PBTA-PS:6TIC, and PBTA-PS ternary devices. It is worth noting that E_g and E_{CT} share the same value in PBTA-PS:6TIC binary and PBTA-PS ternary PSCs, indicative of negligible ΔE_1 in these systems. On the contrary, the ΔE_1 of PBTA-PS:LA1 is 0.19 eV, demonstrating that ΔE_1 is suppressed in the ternary system. Our results illustrate that the ternary system exhibits small energy loss during the charge generation process as the PBTA-PS:6TIC binary system.

To explore the surface and bulk morphologies of the optimal binary and ternary blend films, atomic force microscopy (AFM) and transmission electron microscopy (TEM) measurement were performed. As shown in Figure 5a,b, PBTA-PS:LA1 exhibits a rough surface with a root mean square (RMS) of 4.57 nm and PBTA-PS:6TIC film exhibits a different surface morphology with a RMS of 3.38 nm. After 30% 6TIC is incorporated into the PBTA-PS:LA1 system, the ternary film exhibits a homogeneous surface with a comparable RMS of 4.73 nm. Besides, large grains are not observed, demonstrating a uniform nanoscale morphology (Figure 5c). Meanwhile, as shown

in TEM images, the PBTA-PS:LA1 film exhibits homogeneous bulk morphology. After incorporating 6TIC, the ternary film still exhibits homogeneous morphology with no large aggregates observed. This may be attributed to the good compatibility of acceptors (Figure 5d–f). The good compatibility of acceptors could also be reflected by the phase image based on AFM. After introducing 6TIC to PBTA-PS:LA1 system, the aggregation turned into ordered nanofiber structures (Figure S7, Supporting Information). The appropriate morphology could be beneficial for exciton dissociation and charge transport, leading to high FF.^[55]

The differential scanning calorimeter (DSC) characteristics of LA1, 6TIC, and their blends have been tested to further discuss the compatibility of acceptors. The neat LA1, 6TIC, and LA1:6TIC blend films are prepared by spin-coating. Then the films are scraped and ground to particles for measurements. As shown in Figure S8 in the Supporting Information, the 6TIC shows a sharp exothermic peak during the temperature rising process, which should be attributed to the cold crystallization peak.^[56,57] As for the blend, the cold crystallization peak during the temperature rising process is weakened. Moreover, LA1 exhibits an exothermic peak during the cooling process, which is related to the crystallization peak. However, as for the two acceptors blend, the crystallization peak vanished, and no obvious thermal transition peak was observed during the cooling process, indicating there are no large crystalline grains in the blend.^[58–60] Furthermore, the melting points of LA1, 6TIC, and their blends are obtained by microscopy melting point apparatus. By observing the phase transformation of the particles during the heating process, the melting points are recorded. The melting points of LA1, 6TIC, and their blends are 280, 350, and 255 °C, respectively, which is approximately

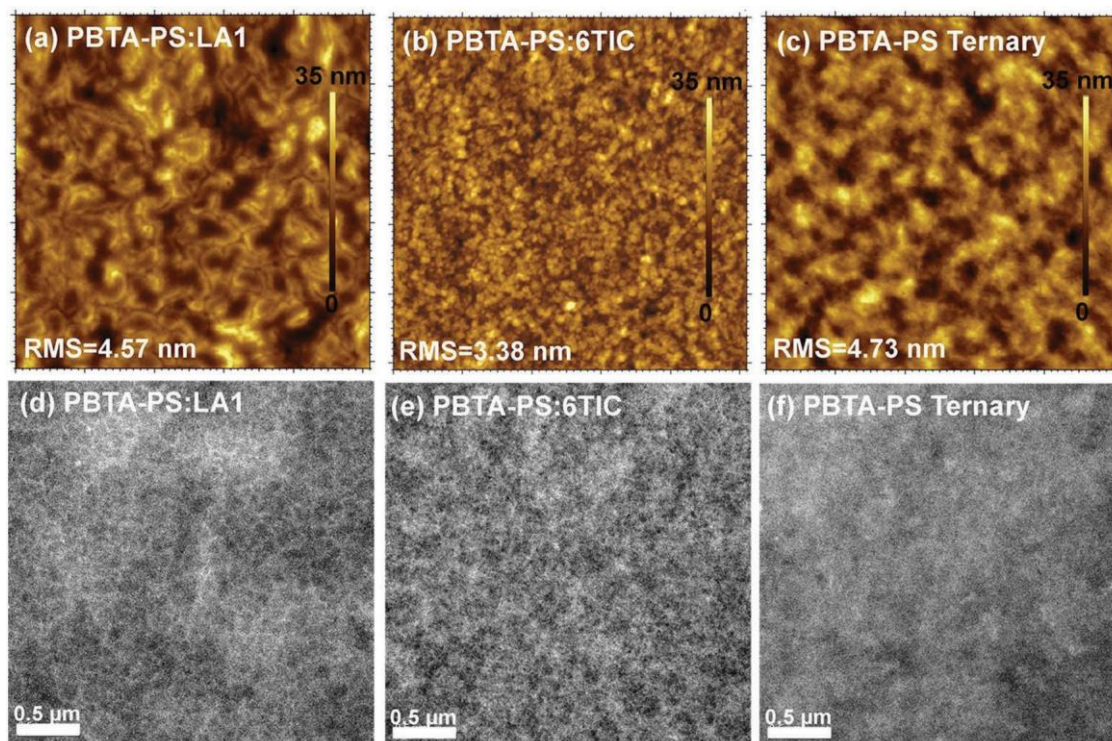


Figure 5. a–c) AFM topography images ($5\ \mu\text{m} \times 5\ \mu\text{m}$); d–f) the respective TEM images of binary blends (PBTA:LA1 and PBTA:6TIC) and the ternary blend under their optimal conditions.

corresponding with the endothermic peak in the DSC graph (Figure S8, Supporting Information). The LA1:6TIC blend film exhibits a decreased melting point. As a conclusion, the miscibility of acceptors could be good enough to construct high-performance ternary PSCs.

The molecular stacking of the optimal binary and ternary blends were further investigated by 2D-GIXD. **Figure 6** shows the 2D-GIXD patterns and the corresponding out of plane and in plane line cuts of blend films. PBTA-PS:LA1 and PBTA-PS:6TIC binary blend exhibit (010) π - π stacking peaks at

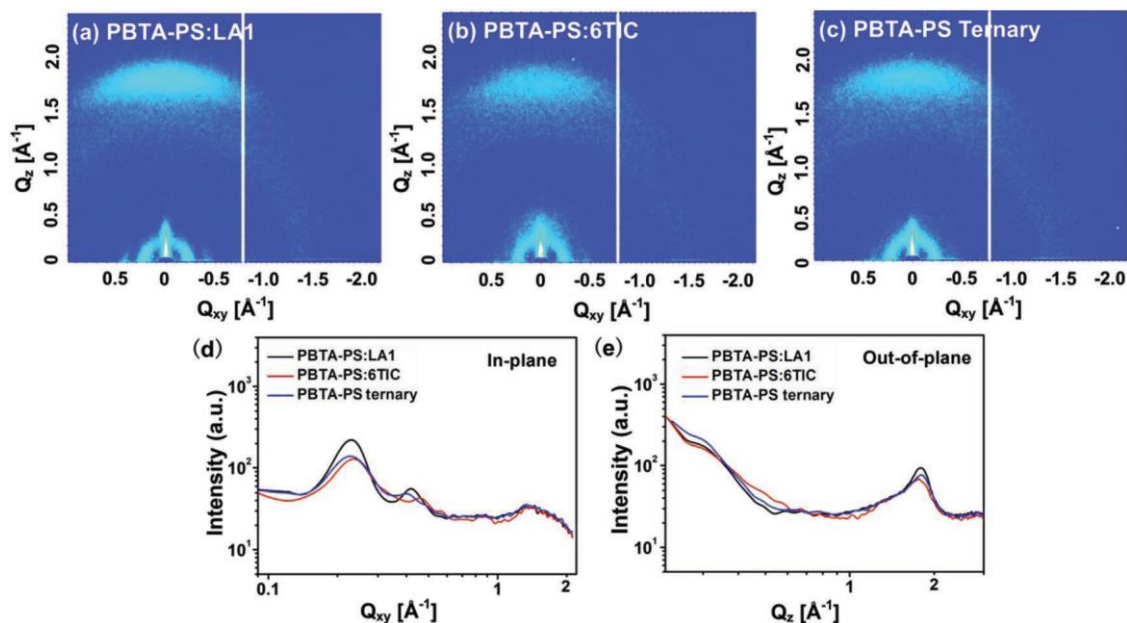


Figure 6. 2D-GIXD scattering patterns of binary blends a) PBTA-PS:LA1 and b) PBTA-PS:6TIC and ternary blend c); the line profiles of 2D-GIXD d) in-plane and e) out-of-plane. The blends were fabricated at their optimal conditions.

$q_z = 1.79$ and 1.77 \AA^{-1} , respectively, indicative of face-on orientation in the two binary systems. The PBTA-PS:6TIC exhibits weak (100) peak in IP direction and (010) peak in OOP direction, which may be attributed to the weak crystallinity of 6TIC. The less-ordered molecular packing may go against the charge transport, leading to weak photo response at 750–900 nm. Compared with the binary systems, the ternary system exhibits moderate (100) peak in IP direction and (010) π - π diffraction peak located at $q_z \approx 1.80 \text{ \AA}^{-1}$ in OOP direction, implying the components may exhibit good miscibility while preserving ordered molecular packing. Moreover, the reserved preferential face-on orientation and optimized molecular packing of the ternary system is highly advantageous for charge transport in the vertical direction, conducive to the improvement of FF and photo response.

The stability of optimal binary and ternary devices has been measured. As shown in Figure S9 in the Supporting Information, the binary and ternary devices could remain over 80% of their original PCEs, over 90% of their original FFs and J_{SC} s, and nearly 95% of their original V_{OC} s after 200 hours, demonstrating good stability of binary and ternary devices.

The impacts of DPE in ternary system are further studied by conducting PL, 2D-GIXD, AFM, and TEM. After adding DPE, the ternary device shows enhanced PL quenching, indicative of enlarged donor-acceptor interface (Figure S5, Supporting Information), which could be beneficial for exciton dissociation. Besides, the ternary blend film with DPE shows enhanced crystallinity in both in-plane and out-of-plane directions, indicating the more ordered molecular stacking. The preferential face-on orientation is not sabotaged by introducing DPE, which could be beneficial for charge transport in the vertical direction (Figure S10, Supporting Information). Moreover, as shown in Figure S11 in the Supporting Information, the ternary blend film with DPE shows more ordered fibriform nanostructures in the surface and a uniform morphology in the bulk with no large grains and aggregates observed, indicating that the addition of DPE did not disturb the miscibility of the components. Based on these evidences, we speculate a schematic diagram of morphology in the ternary film (Figure S12, Supporting Information), demonstrating that the introduction of DPE may help to reach the balance between miscibility and crystallinity, resulting in enhanced device performance.

2. Conclusion

Series of binary and ternary PSCs were fabricated by using PBTA-PS as donor and LA1 and 6TIC as acceptors. The LA1- and 6TIC-based binary devices delivered moderate PCEs of 10.22% and 8.15%, respectively. After incorporating 30% of 6TIC into the LA1 acceptors, the ternary PSC shows an outstanding PCE of 14.24% with a high V_{OC} of 0.84 V, greatly improved J_{SC} of 22.33 mA cm^{-2} , and an excellent FF of 75.94% with DPE as additive. Notably, the outstanding performance of the ternary PSC ranks the best ones among the reported ternary solar cells. The improved device performance could be mainly attributed to the integration of complementary properties including absorption and crystallinity, suppressed energy loss during the charge generation process as well as the energy transfer between the

acceptors. Our results demonstrated that elaborately selecting acceptors with complementary properties is a promising strategy to construct high-performance ternary PSCs.

Supporting Information

Supporting Information is available from the Wiley Online Library or from the author.

Acknowledgements

H.J. and X.L. contributed equally to this work. The authors are deeply grateful to the National Natural Science Foundation of China (51773220, 51573205, 21502205, and 61574064), the Shandong Provincial Natural Science Foundation (ZR2019MF066, ZR2017ZB0314), DICP & QIBEBT (DICP&QIBEBT UN201709), and Dalian National Laboratory for Clean Energy (DNL) CAS for financial support.

Conflict of Interest

The authors declare no conflict of interest.

Keywords

complementary properties, good compatibility, high efficiency, low energy loss, ternary polymer solar cells

Received: May 5, 2019
Revised: June 5, 2019
Published online: June 20, 2019

- [1] G. Li, R. Zhu, Y. Yang, *Nat. Photonics* **2012**, *6*, 153.
- [2] M. Kaltenbrunner, M. S. White, E. D. Głowacki, T. Sekitani, T. Someya, N. S. Sariciftci, S. Bauer, *Nat. Commun.* **2012**, *3*, 770.
- [3] R. Søndergaard, M. Hösel, D. Angmo, T. T. Larsen-Olsen, F. C. Krebs, *Mater. Today* **2012**, *15*, 36.
- [4] J. Liu, S. Chen, D. Qian, B. Gautam, G. Yang, J. Zhao, J. Bergqvist, F. Zhang, W. Ma, H. Ade, O. Inganäs, K. Gundogdu, F. Gao, H. Yan, *Nat. Energy* **2016**, *1*, 16089.
- [5] Q. Wu, D. Zhao, A. M. Schneider, W. Chen, L. Yu, *J. Am. Chem. Soc.* **2016**, *138*, 7248.
- [6] G. Yu, J. Gao, J. C. Hummelen, F. Wudl, A. J. Heeger, *Science* **1995**, *270*, 1789.
- [7] L. Dou, Y. Liu, Z. Hong, G. Li, Y. Yang, *Chem. Rev.* **2015**, *115*, 12633.
- [8] Y. Yang, Z.-G. Zhang, H. Bin, S. Chen, L. Gao, L. Xue, C. Yang, Y. Li, *J. Am. Chem. Soc.* **2016**, *138*, 15011.
- [9] P. Cheng, M. Zhang, T.-K. Lau, Y. Wu, B. Jia, J. Wang, C. Yan, M. Qin, X. Lu, X. Zhan, *Adv. Mater.* **2017**, *29*, 1605216.
- [10] B. Kan, J. Zhang, F. Liu, X. Wan, C. Li, X. Ke, Y. Wang, H. Feng, Y. Zhang, G. Long, R. H. Friend, A. A. Bakulin, Y. Chen, *Adv. Mater.* **2018**, *30*, 1704904.
- [11] Z. Xiao, X. Jia, L. Ding, *Sci. Bull.* **2017**, *62*, 1562.
- [12] H. Ma, H.-L. Yip, F. Huang, A. K. Y. Jen, *Adv. Funct. Mater.* **2010**, *20*, 1371.
- [13] J. Cheng, X. Ren, H. L. Zhu, J. Mao, C. Liang, J. Zhuang, V. A. L. Roy, W. C. H. Choy, *Nano Energy* **2017**, *34*, 76.
- [14] F. Jiang, W. C. H. Choy, X. Li, D. Zhang, J. Cheng, *Adv. Mater.* **2015**, *27*, 2930.

- [15] B. Yang, S. Zhang, S. Li, H. Yao, W. Li, J. Hou, *Adv. Mater.* **2019**, *31*, 1804657.
- [16] S. Dong, K. Zhang, B. Xie, J. Xiao, H.-L. Yip, H. Yan, F. Huang, Y. Cao, *Adv. Energy Mater.* **2019**, *9*, 1802832.
- [17] J. Zhang, B. Kan, A. J. Pearson, A. J. Parnell, J. F. K. Cooper, X.-K. Liu, P. J. Conaghan, T. R. Hopper, Y. Wu, X. Wan, F. Gao, N. C. Greenham, A. A. Bakulin, Y. Chen, R. H. Friend, *J. Mater. Chem. A* **2018**, *6*, 18225.
- [18] W. Xu, F. Gao, *Mater. Horiz.* **2018**, *5*, 206.
- [19] T. Ameri, G. Dennler, C. Lungenschmied, C. J. Brabec, *Energy Environ. Sci.* **2009**, *2*, 347.
- [20] J. Li, Z. Liang, Y. Wang, H. Li, J. Tong, X. Bao, Y. Xia, *J. Mater. Chem. C* **2018**, *6*, 11015.
- [21] T. Ameri, N. Li, C. J. Brabec, *Energy Environ. Sci.* **2013**, *6*, 2390.
- [22] R. Yu, H. Yao, J. Hou, *Adv. Energy Mater.* **2018**, *8*, 1702814.
- [23] T. Liu, L. Huo, X. Sun, B. Fan, Y. Cai, T. Kim, J. Y. Kim, H. Choi, Y. Sun, *Adv. Energy Mater.* **2016**, *6*, 1502109.
- [24] Y. Xie, F. Yang, Y. Li, M. A. Uddin, P. Bi, B. Fan, Y. Cai, X. Hao, H. Y. Woo, W. Li, F. Liu, Y. Sun, *Adv. Mater.* **2018**, *30*, 1803045.
- [25] W. Shen, W. Chen, D. Zhu, J. Zhang, X. Xu, H. Jiang, T. Wang, E. Wang, R. Yang, *J. Mater. Chem. A* **2017**, *5*, 12400.
- [26] Y. Lin, J. Wang, Z.-G. Zhang, H. Bai, Y. Li, D. Zhu, X. Zhan, *Adv. Mater.* **2015**, *27*, 1170.
- [27] W. Chen, G. Huang, X. Li, H. Wang, Y. Li, H. Jiang, N. Zheng, R. Yang, *ACS Appl. Mater. Interfaces* **2018**, *10*, 42747.
- [28] Z. Zhou, S. Xu, J. Song, Y. Jin, Q. Yue, Y. Qian, F. Liu, F. Zhang, X. Zhu, *Nat. Energy* **2018**, *3*, 952.
- [29] W. Zhao, S. Li, S. Zhang, X. Liu, J. Hou, *Adv. Mater.* **2017**, *29*, 1604059.
- [30] R. Lv, D. Chen, X. Liao, L. Chen, Y. Chen, *Adv. Funct. Mater.* **2019**, *29*, 1805872.
- [31] W. Chen, H. Jiang, G. Huang, J. Zhang, M. Cai, X. Wan, R. Yang, *Sol. RRL* **2018**, *2*, 1800101.
- [32] S. M. Menke, N. A. Ran, G. C. Bazan, R. H. Friend, *Joule* **2018**, *2*, 25.
- [33] J. Yuan, W. Guo, Y. Xia, M. J. Ford, F. Jin, D. Liu, H. Zhao, O. Inganäs, G. C. Bazan, W. Ma, *Nano Energy* **2017**, *35*, 251.
- [34] P. Cheng, J. Wang, Q. Zhang, W. Huang, J. Zhu, R. Wang, S.-Y. Chang, P. Sun, L. Meng, H. Zhao, H.-W. Cheng, T. Huang, Y. Liu, C. Wang, C. Zhu, W. You, X. Zhan, Y. Yang, *Adv. Mater.* **2018**, *30*, 1801501.
- [35] M. Zhang, Z. Xiao, W. Gao, Q. Liu, K. Jin, W. Wang, Y. Mi, Q. An, X. Ma, X. Liu, C. Yang, L. Ding, F. Zhang, *Adv. Energy Mater.* **2018**, *8*, 1801968.
- [36] Z. Li, X. Xu, W. Zhang, X. Meng, Z. Genene, W. Ma, W. Mammo, A. Yartsev, M. R. Andersson, R. A. J. Janssen, E. Wang, *Energy Environ. Sci.* **2017**, *10*, 2212.
- [37] X. Ma, W. Gao, J. Yu, Q. An, M. Zhang, Z. Hu, J. Wang, W. Tang, C. Yang, F. Zhang, *Energy Environ. Sci.* **2018**, *11*, 2134.
- [38] H. Zhang, H. Yao, J. Hou, J. Zhu, J. Zhang, W. Li, R. Yu, B. Gao, S. Zhang, J. Hou, *Adv. Mater.* **2018**, *30*, 1800613.
- [39] T. Liu, Z. Luo, Q. Fan, G. Zhang, L. Zhang, W. Gao, X. Guo, W. Ma, M. Zhang, C. Yang, Y. Li, H. Yan, *Energy Environ. Sci.* **2018**, *11*, 3275.
- [40] H. Jiang, X. Li, Z. Liang, G. Huang, W. Chen, N. Zheng, R. Yang, *J. Mater. Chem. A* **2019**, *7*, 7760.
- [41] Y. Li, N. Zheng, L. Yu, S. Wen, C. Gao, M. Sun, R. Yang, *Adv. Mater.* **2019**, *31*, 1807832.
- [42] X. Liao, Z. Yao, K. Gao, X. Shi, L. Zuo, Z. Zhu, L. Chen, F. Liu, Y. Chen, A. K.-Y. Jen, *Adv. Energy Mater.* **2018**, *8*, 1801214.
- [43] Z. Li, W. Zhang, X. Xu, Z. Genene, D. Di Carlo Rasi, W. Mammo, A. Yartsev, M. R. Andersson, R. A. J. Janssen, E. Wang, *Adv. Energy Mater.* **2017**, *7*, 1602722.
- [44] L. Lu, M. A. Kelly, W. You, L. Yu, *Nat. Photonics* **2015**, *9*, 491.
- [45] T. Liu, X. Xue, L. Huo, X. Sun, Q. An, F. Zhang, T. P. Russell, F. Liu, Y. Sun, *Chem. Mater.* **2017**, *29*, 2914.
- [46] K. Akaike, T. Kumai, K. Nakano, S. Abdullah, S. Ouchi, Y. Uemura, Y. Ito, A. Onishi, H. Yoshida, K. Tajima, K. Kanai, *Chem. Mater.* **2018**, *30*, 8233.
- [47] L. Gao, J. Zhang, C. He, Y. Zhang, Q. Sun, Y. Li, *Sci. China: Chem.* **2014**, *57*, 966.
- [48] J. S. Moon, C. J. Takacs, S. Cho, R. C. Coffin, H. Kim, G. C. Bazan, A. J. Heeger, *Nano Lett.* **2010**, *10*, 4005.
- [49] Z. Wang, X. Zhu, J. Zhang, K. Lu, J. Fang, Y. Zhang, Z. Wang, L. Zhu, W. Ma, Z. Shuai, Z. Wei, *J. Am. Chem. Soc.* **2018**, *140*, 1549.
- [50] J. Zhang, R. Xue, G. Xu, W. Chen, G.-Q. Bian, C. Wei, Y. Li, Y. Li, *Adv. Funct. Mater.* **2018**, *28*, 1705847.
- [51] M. Zhang, W. Gao, F. Zhang, Y. Mi, W. Wang, Q. An, J. Wang, X. Ma, J. Miao, Z. Hu, X. Liu, J. Zhang, C. Yang, *Energy Environ. Sci.* **2018**, *11*, 841.
- [52] X. Li, G. Huang, N. Zheng, Y. Li, X. Kang, S. Qiao, H. Jiang, W. Chen, R. Yang, *Sol. RRL* **2019**, *3*, 1900005.
- [53] L. Zuo, X. Shi, S. B. Jo, Y. Liu, F. Lin, A. K.-Y. Jen, *Adv. Mater.* **2018**, *30*, 1706816.
- [54] D. Baran, T. Kirchartz, S. Wheeler, S. Dimitrov, M. Abdelsamie, J. Gorman, R. S. Ashraf, S. Holliday, A. Wadsworth, N. Gasparini, P. Kaienburg, H. Yan, A. Amassian, C. J. Brabec, J. R. Durrant, I. McCulloch, *Energy Environ. Sci.* **2016**, *9*, 3783.
- [55] W. Chen, W. Shen, H. Wang, F. Liu, L. Duan, X. Xu, D. Zhu, M. Qiu, E. Wang, R. Yang, *Dyes Pigm.* **2019**, *166*, 42.
- [56] S. Holliday, R. S. Ashraf, A. Wadsworth, D. Baran, S. A. Yousaf, C. B. Nielsen, C.-H. Tan, S. D. Dimitrov, Z. Shang, N. Gasparini, M. Alamoudi, F. Laquai, C. J. Brabec, A. Salleo, J. R. Durrant, I. McCulloch, *Nat. Commun.* **2016**, *7*, 11585.
- [57] T. J. Aldrich, S. M. Swick, F. S. Melkonyan, T. J. Marks, *Chem. Mater.* **2017**, *29*, 10294.
- [58] T. Kim, J. Choi, H. J. Kim, W. Lee, B. J. Kim, *Macromolecules* **2017**, *50*, 6861.
- [59] K.-H. Kim, H. Kang, H. J. Kim, P. S. Kim, S. C. Yoon, B. J. Kim, *Chem. Mater.* **2012**, *24*, 2373.
- [60] H. Kang, K.-H. Kim, J. Choi, C. Lee, B. J. Kim, *ACS Macro Lett.* **2014**, *3*, 1009.